AIAA JOURNAL
Vol. 45, No. 8, August 2007

Open-Ended Shock Tube Flows: Influence of Pressure Ratio and Diaphragm Position

A. Haselbacher* and S. Balachandar†
University of Florida, Gainesville, Florida 32611
and
S. W. Kieffer‡
University of Illinois at Urbana–Champaign, Urbana, Illinois 61801

DOI: 10.2514/1.23081

The influence of the pressure ratio and the diaphragm location on the flow from open-ended shock tubes is investigated. In contrast to previous studies, in which attention was focused on the discharge of the shock wave from the shock tube, we consider also the influence of the contact discontinuity and the expansion fan. It is found that if the pressure ratio is large enough to lead to supersonic flow behind the contact discontinuity, the flow at the open end relaxes from the conditions behind the contact discontinuity to sonic conditions once the tail of the expansion fan arrives at the open end. Theory indicates that the time scale over which the flow relaxes to sonic conditions is nearly independent of the initial Mach number. Also, the time scale is much longer than that required by the acceleration of subsonic conditions behind the contact discontinuity to sonic conditions. The relaxation process is shown to influence the evolution of the Mach-disk shock, the barrel shock, and the reflected shock wave in an underexpanded jet.

Nomenclature

a	=	speed of sound
d	=	diameter of driver section, $d = 2r_i$
M	=	Mach number
p	=	pressure
r	=	radius
t	=	time
u	=	x component of velocity vector
x	=	spatial coordinate
γ	=	ratio of specific heats
ρ	=	density

Subscripts

B	=	barrel shock
c	=	contact discontinuity
D	=	diaphragm
e	=	expansion
i	=	inner
M	=	Mach-disk shock
o	=	outer
R	=	reflected shock
s	=	shock
v	=	vortex
w	=	wall
1, 2, 3, 4	=	states in shock tube

Superscripts

$*$	=	location downstream of diaphragm

Received 8 February 2006; revision received 24 February 2007; accepted for publication 7 May 2007.

*Assistant Professor, Department of Mechanical and Aerospace Engineering, 222 MAE-B, Post Office Box 116300. Member AIAA.
†Professor, Department of Mechanical and Aerospace Engineering, 231 MAE-A, Post Office Box 116250. Associate Fellow AIAA.
‡Professor, Department of Geology, 245 Natural History Building, MC-102, 1301 West Green Street.

I. Introduction

THE shock tube has proven an exceptionally valuable tool for the study of physical and chemical processes, see, e.g., Bradley [1] and Gaydon and Hurle [2]. In its simplest form, the shock tube consists of a long cylinder of circular or square cross section in which a diaphragm separates the driver section occupied by a gas at high pressure from the driven section occupied by a gas at lower pressure. The sudden bursting of the diaphragm produces a shock wave and contact discontinuity which propagate into the driven section and an expansion wave which propagates into the driver section.

Shock tubes with a change in the cross-sectional area at the diaphragm location can also be considered. Such shock tubes are said to have positive or negative chambrage if the cross-sectional area of the driver section is larger or smaller than that of the driven section, respectively, (see, e.g., Glass and Sislian [3]). The primary motivation for considering shock tubes with positive chambrage is to increase the shock strength, see, e.g., Alpher and White [4], Sugiyama [5], and Emanuel et al. [6]. In this article, we consider open-ended shock tubes in which the driven section contains an abrupt area expansion, such as that shown in Fig. 1. These configurations may be viewed as shock tubes with negative chambrage in which the location at which the cross-sectional area expands does not coincide with the location of the diaphragm. Such configurations are sometimes referred to as expansion tubes, but we will reserve this designation for the case in which the cross-sectional area of the expansion section is finite and the walls of the expansion section play a role over the time of interest. In contrast, we use the term open-ended shock tube if the size of the domain downstream of the expansion is either infinite or so large that its precise size is not important over the time of interest.

Open-ended shock tubes have been used in many experimental studies of the discharge of weak or strong shock waves from ducts. For example, Kim and Setoguchi [7] and Kim et al. [8] used open-ended shock tubes to investigate the formation of compression waves at the exit of train tunnels. Blast-wave phenomena related to gun discharges were investigated by Phan and Stollery [9] and Schmidt and Duffy [10].

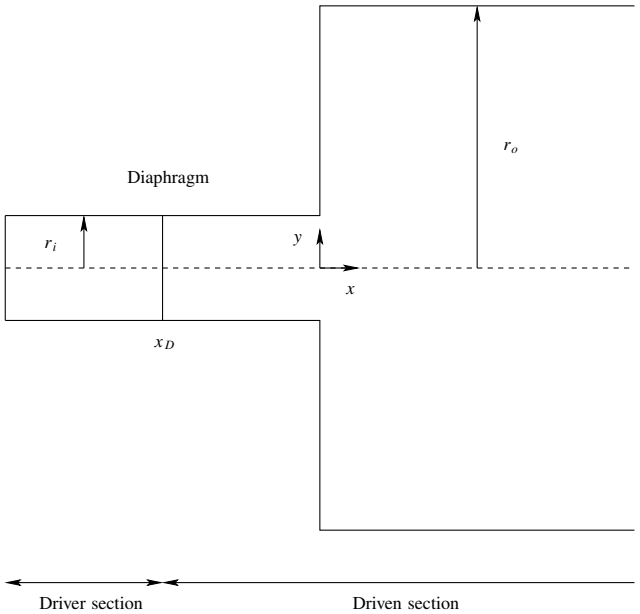

Fig. 1 Schematic overview of open-ended shock-tube geometry considered in this work.

The flow from open-ended shock tubes can be described qualitatively in relatively simple fashion. For simplicity, this description assumes a planar geometry. On reaching the open end at $t_0 = -x_D/(M_s a_1)$, the shock wave will diffract at the corners, where M_s is the shock Mach number and a_1 is the speed of sound in the driven section. The diffraction process is self-similar until the expansion waves generated at the corners reach the centerline of the shock tube at $t - t_0 \approx r_i/a_2$, where a_2 is the speed of sound behind the shock wave. Provided the flow behind the shock wave is supersonic, the state at the open end is constant until the contact discontinuity arrives. Otherwise, expansion waves travel upstream into the shock tube and accelerate the flow until sonic conditions are established at the open end. The upstream propagation of expansion waves following the arrival of the shock wave has been studied by Rudinger [11,12].

The flow behind the shock wave separates at the corners, leading to vortex sheets which roll up into vortices. The flow development after the initial stages of diffraction depends on the expansion $r_o - r_i$, the shock Mach number M_s, and the speed of sound a_1 of the driven section. For $t - t_0 \ll (r_o - r_i)/(M_s a_1)$, the boundaries of the expanded section do not play an important role and the configuration can be considered open-ended. In this case, an underexpanded jet forms at the open end of the shock tube, see, e.g., Adamson and Nicholls [13] and Bier and Schmidt [14]. However, over sufficiently long time, i.e., $t - t_0 \gtrapprox (r_o - r_i)/(M_s a_1)$, the flow is influenced by the walls of the expansion section and the configuration must be considered as an expansion tube. In expansion tubes, the shock wave reflected from the walls of the expansion section interacts with the vortex sheet, vortex, and itself to produce very complicated flow patterns.

This rich set of flow features has made open-ended shock tubes a widely studied configuration. The diffraction of shock waves at corners was studied theoretically by Whitham [15], experimentally by Skews [16,17], and numerically by Hillier [18,19], among many others. Baird [20] investigated experimentally the creation and evolution of vortex rings. Sun and Takayama [21] demonstrated that the vortex sheet outweighs baroclinic effects in producing vorticity behind the shock wave. Chang and Kim [22] and Jiang et al. [23] considered the interactions between the various flow features in expansion tubes. Yu and Grönig [24] studied open-ended shock tubes with the aim of reducing the attenuation through modifying the shape of the open end.

In the preceding description of flow produced in open-ended shock tubes, the flow behind the contact discontinuity was not addressed. Indeed, most experimental and numerical investigations do not mention the contact discontinuity. In theory, provided the open end is located far away from the diaphragm, the contact discontinuity will be lagging the shock wave by a substantial distance, and therefore steady postshock conditions of some duration can be established. (In practice, perfectly steady conditions cannot be achieved because of boundary-layer growth on the shock-tube walls, see, e.g., Gaydon and Hurle [2].) Including the contact discontinuity and expansion fan in the studies of the flow from open-ended shock tubes leads to interesting effects, in particular if the shock-tube pressure ratio is relatively large and if the diaphragm is close enough to the open end so that the steady postshock conditions are of limited duration.

The main goal of the present article is to investigate analytically and numerically the effects of the shock-tube pressure ratio and the diaphragm position on the flow from open-ended shock tubes. To this end, the Euler equations are solved using the method described by Haselbacher [25]. It will be shown that additional unsteady effects can arise provided the diaphragm is not located at the open end and the pressure ratio is large enough for supersonic conditions to exist behind the contact discontinuity.

The remainder of this paper is structured as follows: In Sec. II, the theory of closed shock tubes is summarized, the conditions for supersonic flow behind the contact discontinuity are explored, the additional unsteady effects are analyzed, and their relevance to open-ended shock tubes is discussed. Numerical results for shock wave diffraction at a corner are compared with Whitham's theory and the experiments of Skews [16,17] in Sec. III. Highly resolved computations of flows from open-ended shock tubes are presented in Sec. IV for both low- and high-pressure ratios and two diaphragm positions. Detailed comparisons with the experimental data of Bier and Schmidt [14] are shown. Particular attention is focused on the evolution of the flow at the open end which exhibits excellent agreement with the theory presented in Sec. II.

II. Review of Shock-Tube Theory

A. Closed Shock Tubes

Here we briefly review the theory of flows in closed shock tubes, with particular focus on conditions behind the contact discontinuity, because this aspect of the flow will be relevant to subsequent discussions of open-ended shock tubes. Throughout, it is assumed that $x \gtrless 0$ represents the driver and driven sections, respectively.

1. Basic Theory

The flow in shock tubes can be divided into two distinct cases. The first case arises when the flow behind the contact discontinuity is subsonic. The expansion fan is then contained entirely within the driver section. The second case occurs when the flow behind the contact discontinuity is supersonic. Then the head of the expansion fan travels into the driver section while the tail travels into the driven section. In the following, the subscripts 1–4 indicate the uniform flow conditions in the driven section, behind the shock wave/ahead of the contact discontinuity, behind the contact discontinuity/ahead of the expansion fan, and in the driver section, respectively. Reflections of the expansion and shock waves and their subsequent interactions with the contact discontinuity and each other are ignored. Furthermore, it is assumed that $u_1 = u_4 = 0$.

A nonlinear equation for the shock wave Mach number M_s (the so-called shock-tube equation) can be derived from the condition that the pressure is constant across the contact discontinuity, see, e.g., Owczarek [26]. Once the Mach number of the shock wave is computed, the Mach numbers of the flows behind the shock wave and behind the contact discontinuity can be computed. The expression for the Mach number behind the contact discontinuity is

$$M_3 = \frac{2}{\gamma_4 - 1}\left[\frac{\gamma_1 + 1}{\gamma_4 - 1}\frac{a_4}{a_1}\frac{M_s}{M_s^2 - 1} - 1\right]^{-1} \tag{1}$$

The behavior of the three Mach numbers as a function of p_4/p_1 and a_4/a_1 is shown in Fig. 2, assuming that $\gamma_1 = \gamma_4 = 1.4$. It can be seen that the Mach numbers of the shock wave and the flow behind

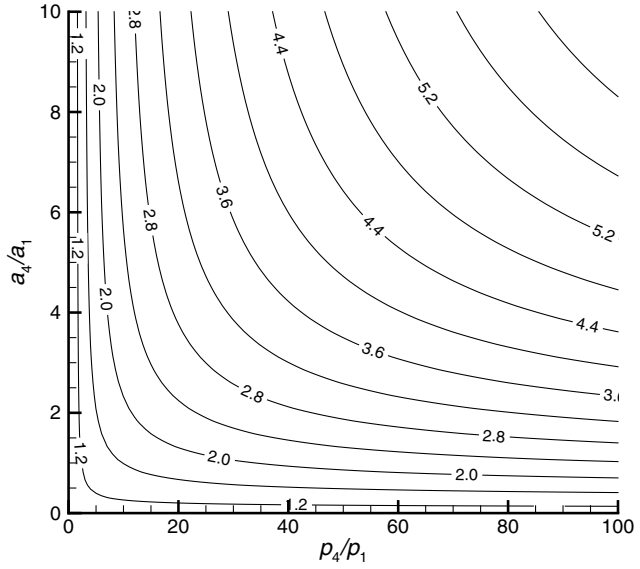

a) M_s

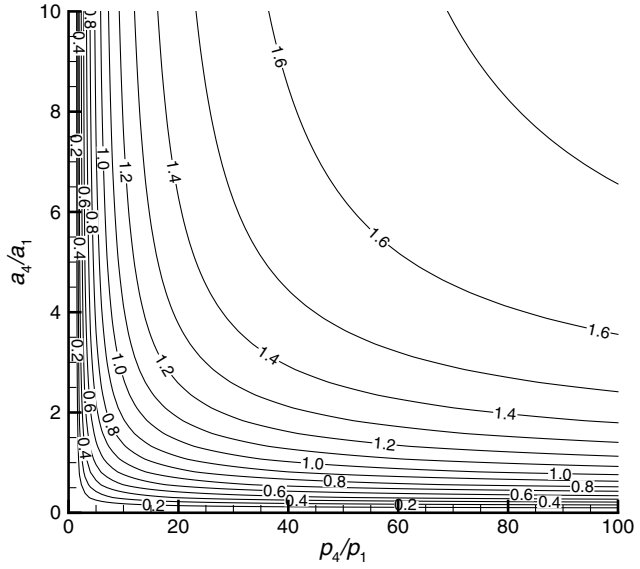

b) M_2

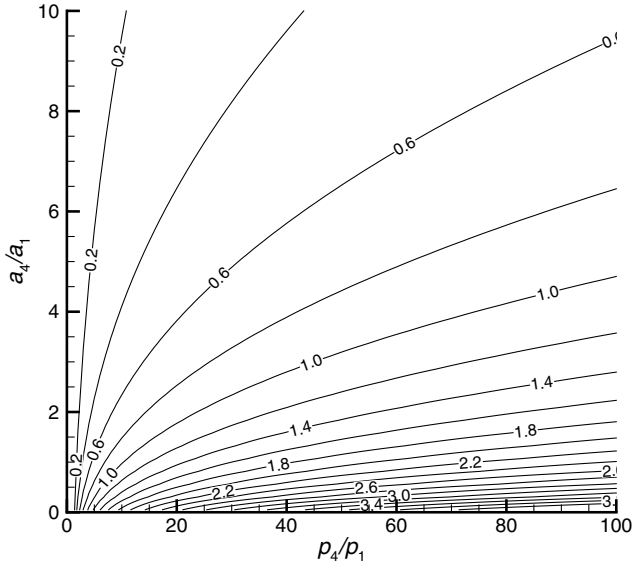

c) M_3

Fig. 2 Mach numbers in shock tube as a function of p_4/p_1 and a_4/a_1 for $u_1 = u_4 = 0$ and $\gamma_1 = \gamma_4 = 1.4$.

the shock wave increase with increasing p_4/p_1 and a_4/a_1, whereas the Mach number of the flow behind the contact discontinuity increases with increasing p_4/p_1 and decreasing a_4/a_1. Thus, supersonic conditions behind the contact discontinuity are established for a combination of large p_4/p_1 and sufficiently small a_4/a_1.

2. *Flow Behind Contact Discontinuity*

It is of some interest to investigate in more detail the flow behind the contact discontinuity, in particular, to establish conditions under which supersonic flow is produced. These conditions do not receive much attention in standard texts and the literature. Attention is usually focused on the flow behind the shock wave and its reflection from the end wall of the driven section. The brief discussion by Owczarek [26] is a notable exception. In the following, we expand on this discussion and establish and investigate in detail the conditions for supersonic flow behind the contact discontinuity.

Equation (1) can be solved for the shock wave Mach number which yields sonic conditions behind the contact discontinuity,

$$M_s|_{M_3=1} = \frac{1}{2}\frac{\gamma_1+1}{\gamma_4+1}\frac{a_4}{a_1} + \sqrt{1+\left(\frac{1}{2}\frac{\gamma_1+1}{\gamma_4+1}\frac{a_4}{a_1}\right)^2} \tag{2}$$

and substituting this relation into the shock-tube equation gives, for a given speed-of-sound ratio a_4/a_1, the pressure ratio p_4/p_1 required to produce sonic conditions behind the contact discontinuity,

$$\left.\frac{p_4}{p_1}\right|_{M_3=1} = \left(\frac{\gamma_4+1}{2}\right)^{2\gamma_4/\gamma_4-1}\left\{1+\frac{\gamma_1}{\gamma_1+1}\left(\frac{\gamma_1+1}{\gamma_4+1}\frac{a_4}{a_1}\right)^2 \times\left[1+\sqrt{1+4\left(\frac{\gamma_4+1}{\gamma_1+1}\frac{a_1}{a_4}\right)^2}\right]\right\} \tag{3}$$

Equation (3) describes the $M_3 = 1$ curve in Fig. 2c. Values of the pressure ratio which are larger or smaller than the right-hand side of Eq. (3) produce supersonic or subsonic flow behind the contact discontinuity, respectively.

Having established the conditions for supersonic flow to exist behind the contact discontinuity, we now turn our attention to the evolution of the flow behind the contact discontinuity. For supersonic flow behind the contact discontinuity, it is simple to show that sonic conditions are established at $x = 0$ and hence the solution there remains constant in time.

The propagation of the expansion fan into the driven section means that the flow properties at a location $x^* > 0$ will undergo a continuous variation after the arrival of the expansion fan in addition to the two discontinuous changes when the shock wave and contact discontinuity arrive, see Fig. 3. The arrival times of the shock wave, contact discontinuity, and the expansion fan are given by $t_s = x^*/(M_s a_1)$, $t_c = x^*/u_2$, and $t_e = x^*/(u_3 - a_3)$, where u_3 and a_3 can be determined from a_1, a_4, M_s, and M_3 using standard shock wave and expansion-fan relationships.

For a given location $x^* > 0$, the variation of flow properties within the expansion fan for $t > t_e$ can be determined easily. For example, the Mach number variation can be expressed in terms of the time after the arrival of the expansion fan $t^* = t - t_e$ as

$$M^* = M(x^*, t^*) = \frac{M_3 + \alpha(a_3 t^*/x^*)}{1 + \alpha(a_3 t^*/x^*)} \tag{4}$$

where

$$\alpha = \frac{2}{\gamma_4+1}(M_3 - 1)\left(1 + \frac{\gamma_4 - 1}{2}M_3\right) \tag{5}$$

As expected, $M(x^*, 0) = M_3$, corresponding to the condition behind the contact discontinuity. The longtime asymptotic is given by the sonic condition, i.e., $M(x^*, t^* \to \infty) = 1$. Note that only at the location of the diaphragm does the Mach number remain sonic at all times. At all other points, the Mach number will relax from M_3 to the

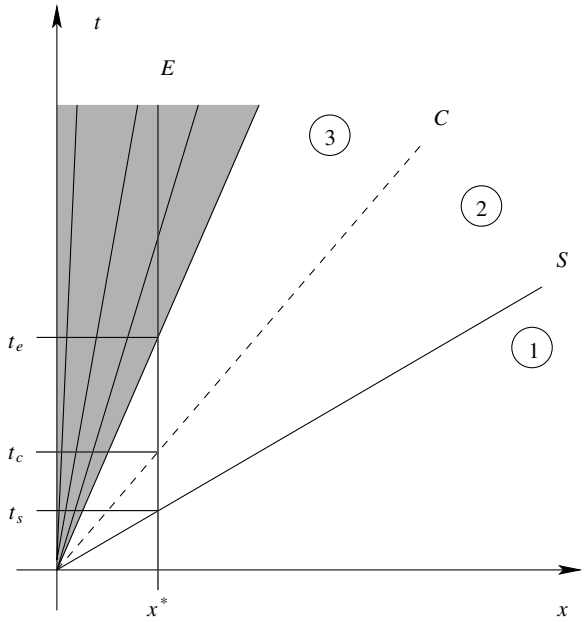

Fig. 3 Definition of arrival times of shock wave, contact discontinuity, and expansion fan at location x^*.

sonic condition over a period of time, thereby introducing an unsteady effect beyond those caused by the passages of the shock wave and contact discontinuity.

Using Eq. (4), the evolution of the Mach number at a location $x^* > 0$ for supersonic flow behind contact discontinuity can be determined. For the initial conditions $p_4/p_1 = 50$, $\rho_4/\rho_1 = 28.74$, $u_1 = u_4 = 0$, and $\gamma_4 = \gamma_1 = 1.4$, the evolution of the Mach number at $x^* = 1$ is shown in Fig. 4a. The passage of the shock wave and contact discontinuity can be seen clearly, as well as the initial stages of the relaxation when the tail of the expansion fan arrives.

The time scale of this relaxation is dependent on x^*. In the limit of $x^* \to 0$ the time scale approaches zero and the sonic condition is attained immediately. Equation (4) can be rearranged to give an expression for the nondimensional time variable

$$\frac{a_3 t^*}{x^*} = \frac{1}{\alpha}\frac{M_3 - M^*}{M^* - 1} \tag{6}$$

which gives the time t^* for the Mach number at x^* to decrease from M_3 to M^*. A plot of Eq. (6) is given in Fig. 4b for several values of M_3. It can be seen that the nondimensional time scale during which the flow relaxes to near-sonic conditions remains of $\mathcal{O}(10)$ independent of M_3. The time required by M^* to decrease from M_3 to $1 + \delta$, where $\delta \ll 1$, can be estimated as

$$t^*|_{M^*=1+\delta} = \frac{\gamma_4 + 1}{2\{1 + [(\gamma_4 - 1)/2]M_3\}}\frac{x^*}{a_3\delta} \tag{7}$$

where it was assumed that $M_3 \gg 1$. Hence, it is clear that the duration of unsteadiness is linearly dependent on x^* and inversely dependent on a_3 and δ.

The corresponding temporal variation in the expansion fan of other flow properties can be computed analogously. For example, the pressure varies according to

$$\frac{p^*}{p_3} = \left(\frac{1 + \alpha(a_3 t^*/x^*)}{1 + (M_3 - 1)(a_3 t^*/x^*)}\right)^{2\gamma_4/\gamma_4 - 1} \tag{8}$$

It can be shown from Eq. (8) that as $t^* \to \infty$,

$$\frac{p^*}{p_4} = \left(\frac{2}{\gamma_4 + 1}\right)^{2\gamma_4/\gamma_4 - 1} \tag{9}$$

i.e., p^* is the pressure attained when the properties at state 4 are accelerated to sonic conditions.

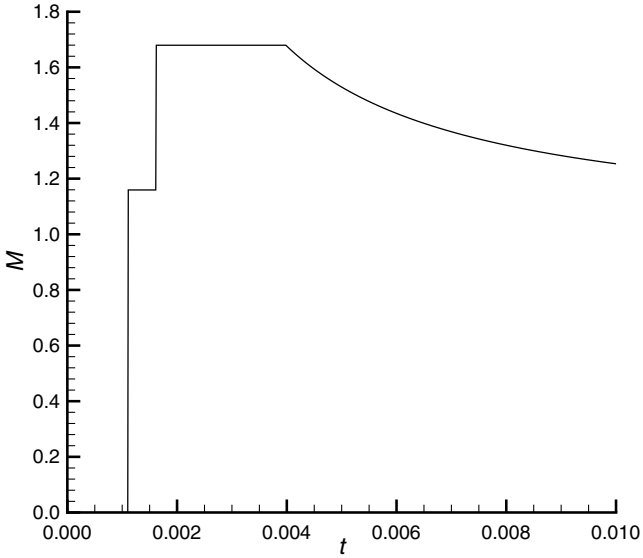

a) Mach number at $x^* = 1$ for $p_4/p_1 = 50$, $\rho_4/\rho_1 = 28.74$, $u_1 = u_4 = 0$, and $\gamma_4 = \gamma_1 = 1.4$

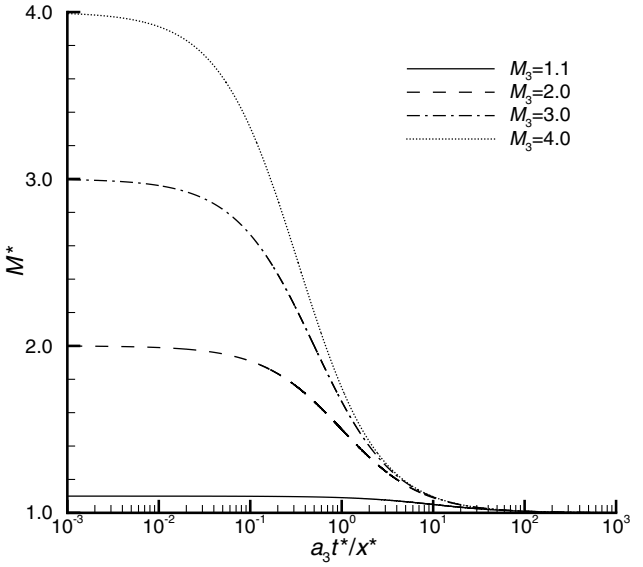

b) Nondimensional time required for Mach number at $x*$ to drop from M_3 to M^* for $u_1 = u_4 = 0$ and $\gamma_1 = \gamma_4 = 1.4$

Fig. 4 Evolution of Mach number at location $x^* > 0$ for supersonic flow behind contact discontinuity.

It is worth noting that a figure similar to Fig. 4a was shown by Rudinger [27] in 1949. In discussing the use of shock tubes as intermittent supersonic wind tunnels, Rudinger pointed out, apparently for the first time, that the Mach number behind the contact discontinuity could be larger than that behind the shock wave. However, Rudinger did not address the relaxation of flow properties investigated in this section.

B. Open-Ended Shock Tubes

The flow from open-ended shock tubes was described qualitatively in the Introduction. A comprehensive analytical description of the entire flowfield is not possible because of the discontinuities and the multidimensional nature of the flow once it emanates from the open end. Useful results can be obtained from theoretical studies, however, if attention is focused on specific portions or features of the flowfield.

Such theoretical studies need to distinguish between subsonic or supersonic flow behind the shock wave and contact discontinuity.

The following discussion is focused on the cases in which the Mach numbers behind the shock wave and contact discontinuity are either both subsonic or both supersonic. The diffraction of the shock wave, which is not influenced by this distinction, was investigated theoretically by Whitham [15].

1. Subsonic Flow Behind Shock Wave and Contact Discontinuity

Rudinger [11,12] analyzed the interaction of a shock wave with the open end of a duct based on acoustic theory. The resulting expansion wave which propagates upstream is in general not centered. The expansion wave is refracted at the contact discontinuity, leading to a transmitted expansion wave and a reflected wave, which may be either an expansion wave or compression waves which steepen into a shock wave, as demonstrated by Billington and Glass [28]. It can be shown that the transmitted expansion wave is always stronger than the incident expansion wave. The reflected expansion wave or shock wave will again be reflected from the open end, setting up a complicated interaction pattern. Because the main focus of this article is on the flow from open-ended shock tubes when the pressure ratio is large, the subsonic case is not analyzed in detail.

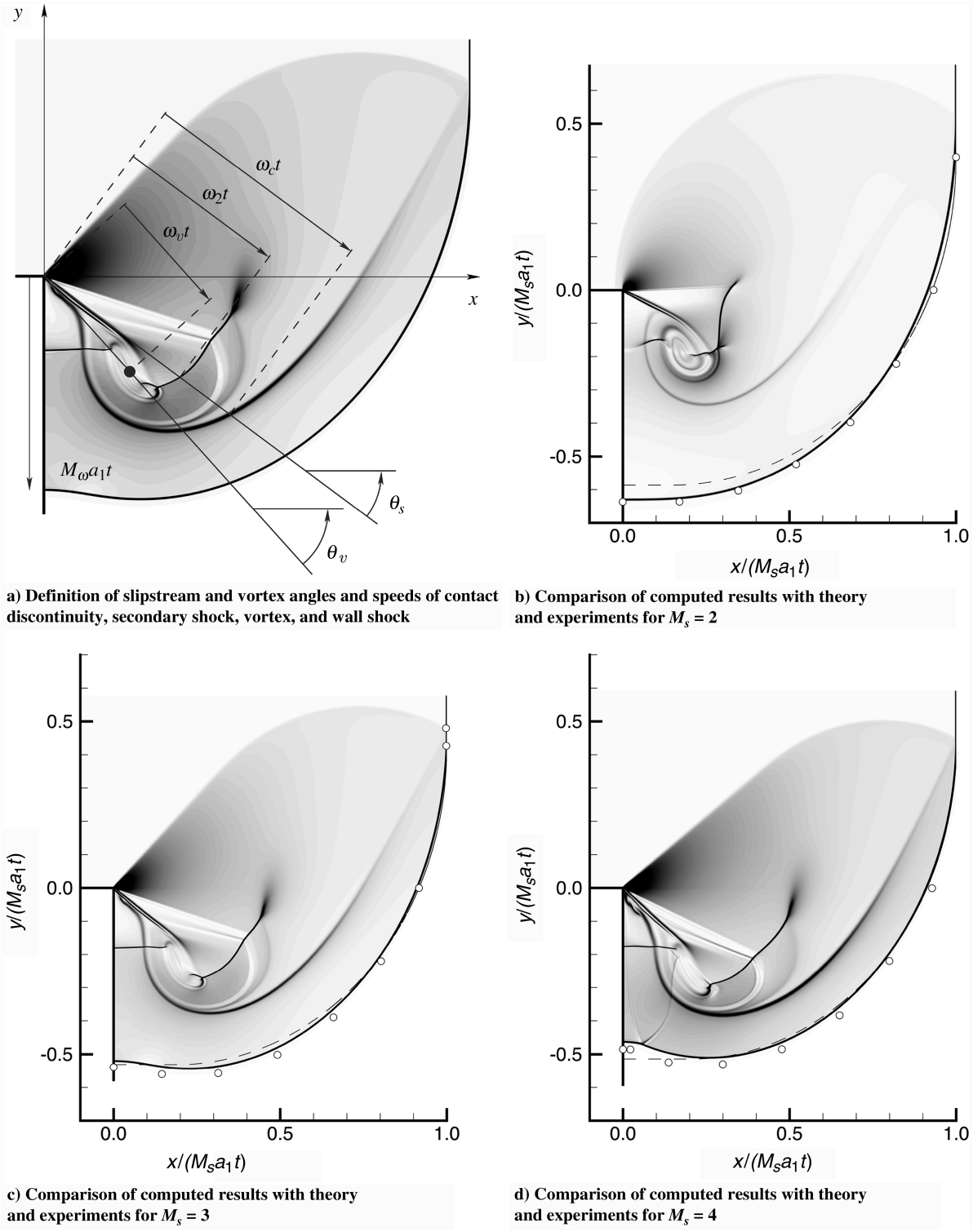

a) Definition of slipstream and vortex angles and speeds of contact discontinuity, secondary shock, vortex, and wall shock

b) Comparison of computed results with theory and experiments for $M_s = 2$

c) Comparison of computed results with theory and experiments for $M_s = 3$

d) Comparison of computed results with theory and experiments for $M_s = 4$

Fig. 5 Definition of quantities to be compared and comparisons of computed results with theory of Whitham [15] (dashed lines) and experiments of Skews [16] (symbols).

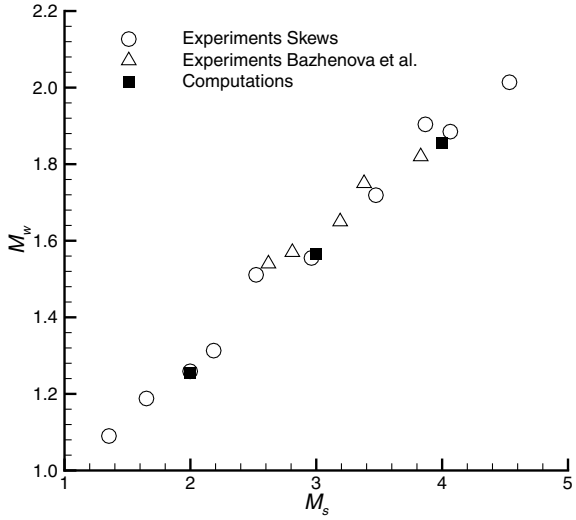

a) Mach number of wall shock

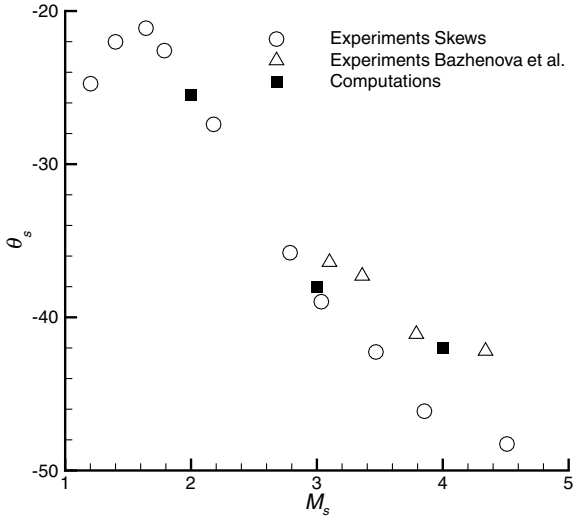

b) Slip-stream angle

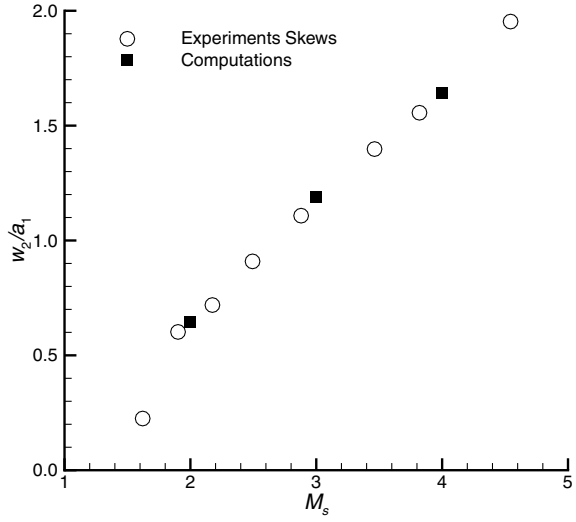

c) Mach number of secondary shock

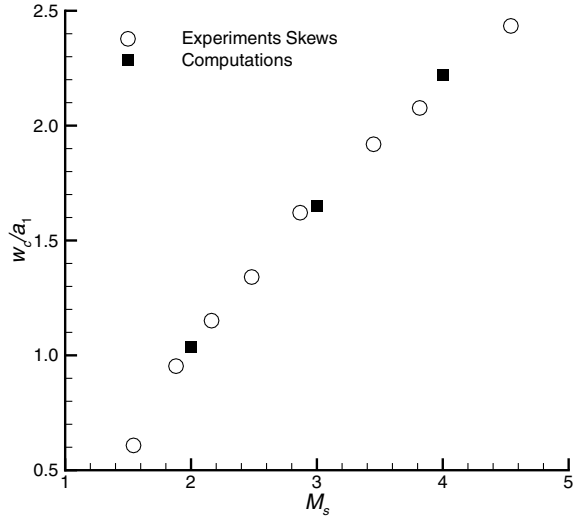

d) Mach number of contact discontinuity

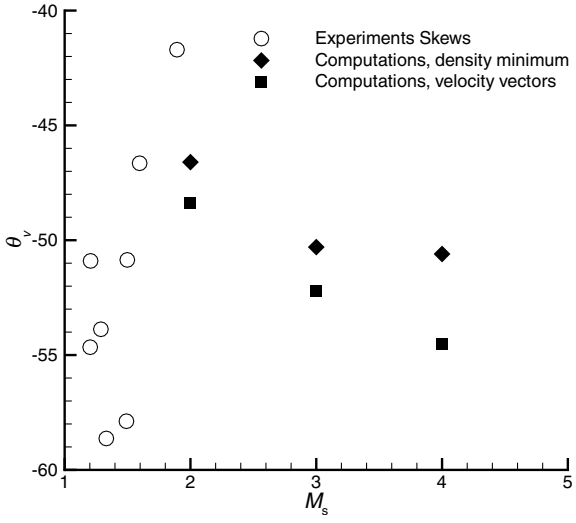

e) Vortex angle

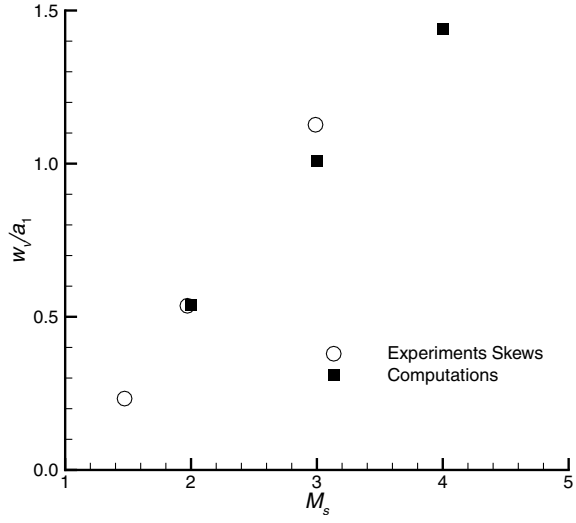

f) Mach number of vortex

Fig. 6 Comparison of computed quantities with experiments for shock diffraction.

Table 1 Summary of initial conditions for open-ended shock tubes cases. All cases use $u_1 = u_4 = 0$ and $\gamma_1 = \gamma_4 = 1.4$

p_4/p_1	ρ_4/ρ_1	x_D/d
7.25	6.58	−1.0
50.0	28.74	−1.0
50.0	28.74	0.0

2. Supersonic Flow Behind Shock Wave and Contact Discontinuity

If the flow behind the shock wave and contact discontinuity is supersonic, then the evolution of the flow at the open end can be determined from the evolution of the flow in a closed shock tube at a location x^* downstream of the diaphragm as presented in Sec. II.A.1. As already discussed, supersonic flow behind the contact discontinuity introduces an unsteadiness into the conditions at the open end. As the conditions at the open end determine the nature and evolution of the jet issuing from the shock tube, it must be expected that the evolution of jets from open-ended shock tubes for which the pressure ratio is large enough to produce supersonic flow behind the contact discontinuity will undergo additional transients.

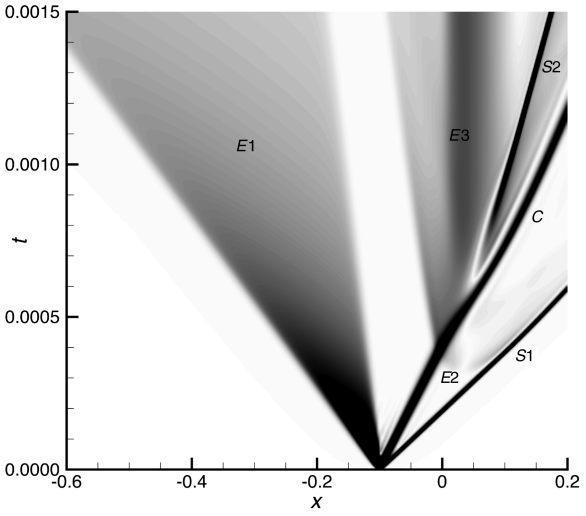

Fig. 8 Numerically generated $x - t$ diagram of flow along centerline of open-ended shock tube for $p_4/p_1 = 7.25$, $\rho_4/\rho_1 = 6.58$.

III. Validation: Shock Diffraction at a Corner

Skews [16,17] presented detailed measurements of the diffraction of shock waves of different Mach numbers in air for various corner angles. As explained in the preceding section, the flow from an open-ended shock tube is characterized initially by the diffraction of the shock wave. For this reason, the experiments of Skews are quite relevant to the present investigation of the flow from open-ended shock tubes.

In the following, we will compare the computational results with the experimental measurements of Skews [16,17] for shock Mach numbers of $M_s = 2$, 3, and 4. The computational domain may be thought to represent the region around the corner $(x, y) = (0, -r_i)$ shown in Fig. 1. The computations are carried out on hexahedral grids with a uniform spacing of $\Delta x = \Delta y = 0.001$ and a single cell in the z direction. No fluxes are computed for the boundaries with normals in the positive or negative z directions. Characteristic inflow boundary conditions are imposed which are consistent with the state behind the shock wave for a given Mach number. The gas constant and ratio of specific heats are assumed to be $R = 287.04$ J/(kg K) and 1.4, respectively.

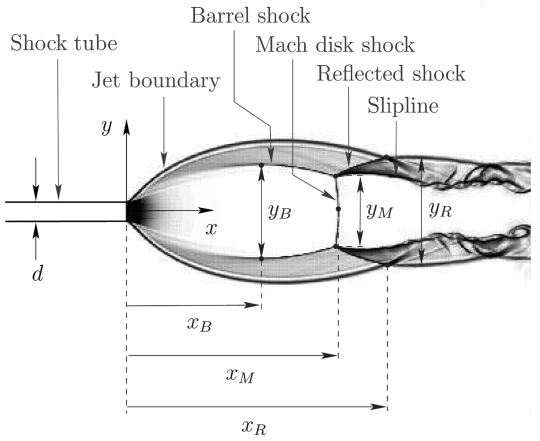

Fig. 9 Definition of flow features and streamwise position and cross-streamwise extents of barrel shock, Mach-disk shock, and reflected shock.

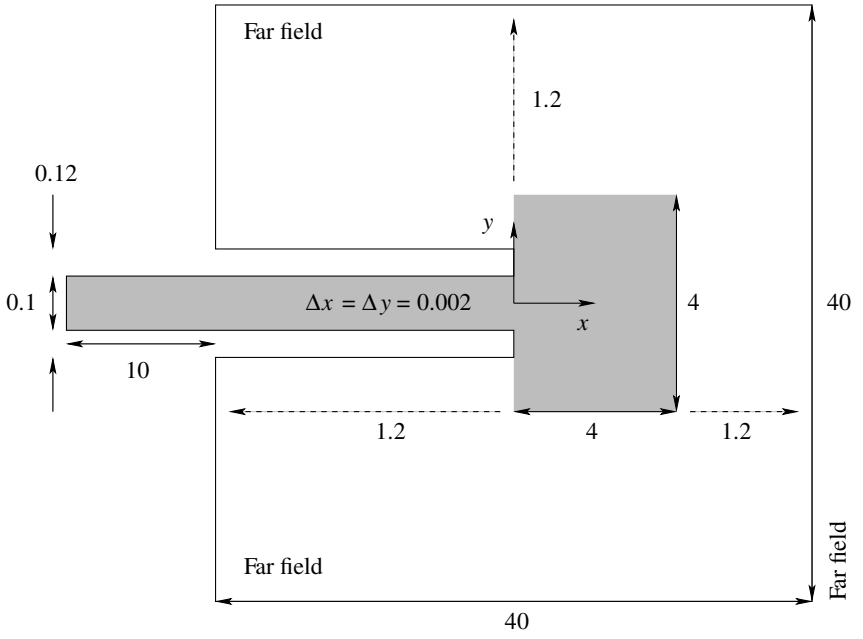

Fig. 7 Computational domain and boundary conditions used for open-ended shock-tube cases. Not drawn to scale.

The initial condition for all computations is a perfectly sharp shock profile at $x = -0.35$. It is well known that the use of a sharp initial shock profile leads to spurious shear and entropy waves, as first noticed by Glaz et al. [29]. In the present case, these waves interact with the flow features behind the diffracted shock wave and corrupt the numerical solution. To prevent this interaction, the computation is interrupted just before the shock wave reaches the corner and the solution behind the shock wave is reinitialized to a uniform state. The computation is then restarted with the reinitialized solution.

In addition to comparing the computational results with the experiments of Skews [16,17], comparisons with the measurements of Bazhenova et al. [30], performed in nitrogen, will also be made. This comparison is justified because air is mostly nitrogen.

In the results to be presented, t is defined to be the time elapsed after the shock reached the corner. The definitions of the quantities to be compared are depicted in Fig. 5a. The shock profiles are presented in normalized coordinates $x/(M_s a_1 t)$ and $y/(M_s a_1 t)$ in Figs. 5b–5d for the three initial shock Mach numbers. At all Mach numbers, the

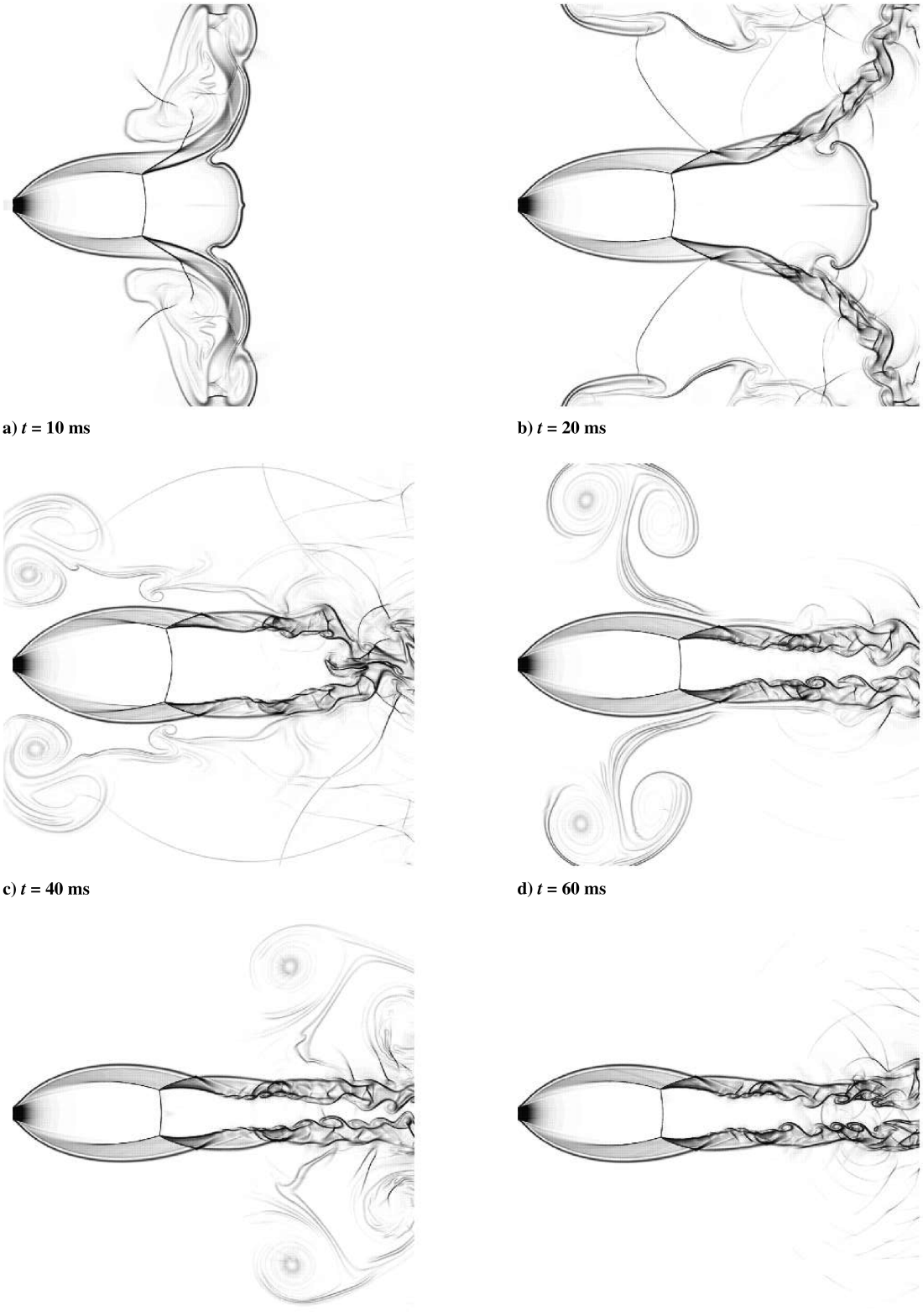

a) t **= 10 ms** **b)** t **= 20 ms**

c) t **= 40 ms** **d)** t **= 60 ms**

e) t **= 80 ms** **f)** t **= 100 ms**

Fig. 10 Development of flow for $p_4/p_1 = 50$, $\rho_4/\rho_1 = 28.74$, and $x_D/d = -1$.

diffracted shock, the contact discontinuity, the secondary shock, the slip stream, the vortex, and the tertiary shock are captured crisply and compare well with the results presented by Hillier [18]. More specifically, at $M_s = 4$, the kink in the diffracted shock near the wall and the roll-up instability of contact discontinuity near the corner are well captured. For comparison, the shock profiles measured by Skews [16] and predicted by the theory of Whitham [15] are also shown. The comparison between the computed and measured shock profiles is in general excellent, in particular for $M_s = 2$. For $M_s = 3$ and 4, the computed shock waves appear to lag those observed by Skews [16]. The lag observed in the computed shock wave may be caused at the early stages of diffraction, where the neglect of viscosity may have an impact, because the computed wall shock Mach numbers compare very well with those measured by Skews, as shown in Fig. 6a.

The angle of the slipstream is compared with the experiments of Skews in Fig. 6b. For $M_s = 2$ and 3, the agreement is very good, but for $M_s = 4$ the computed angle is larger than that measured by Skews [16]. The discrepancy may perhaps be due to uncertainties in the measurements, as the comparison with the experiments of Bazhenova et al. [30] is significantly better. The results of Hillier [18] also exhibit better agreement with the experiments of Bazhenova et al. [30] for higher Mach numbers. The computed Mach numbers of the secondary shock and contact discontinuity are compared with the experiments of Skews [16] in Figs. 6c and 6d. The agreement is very good for all Mach numbers.

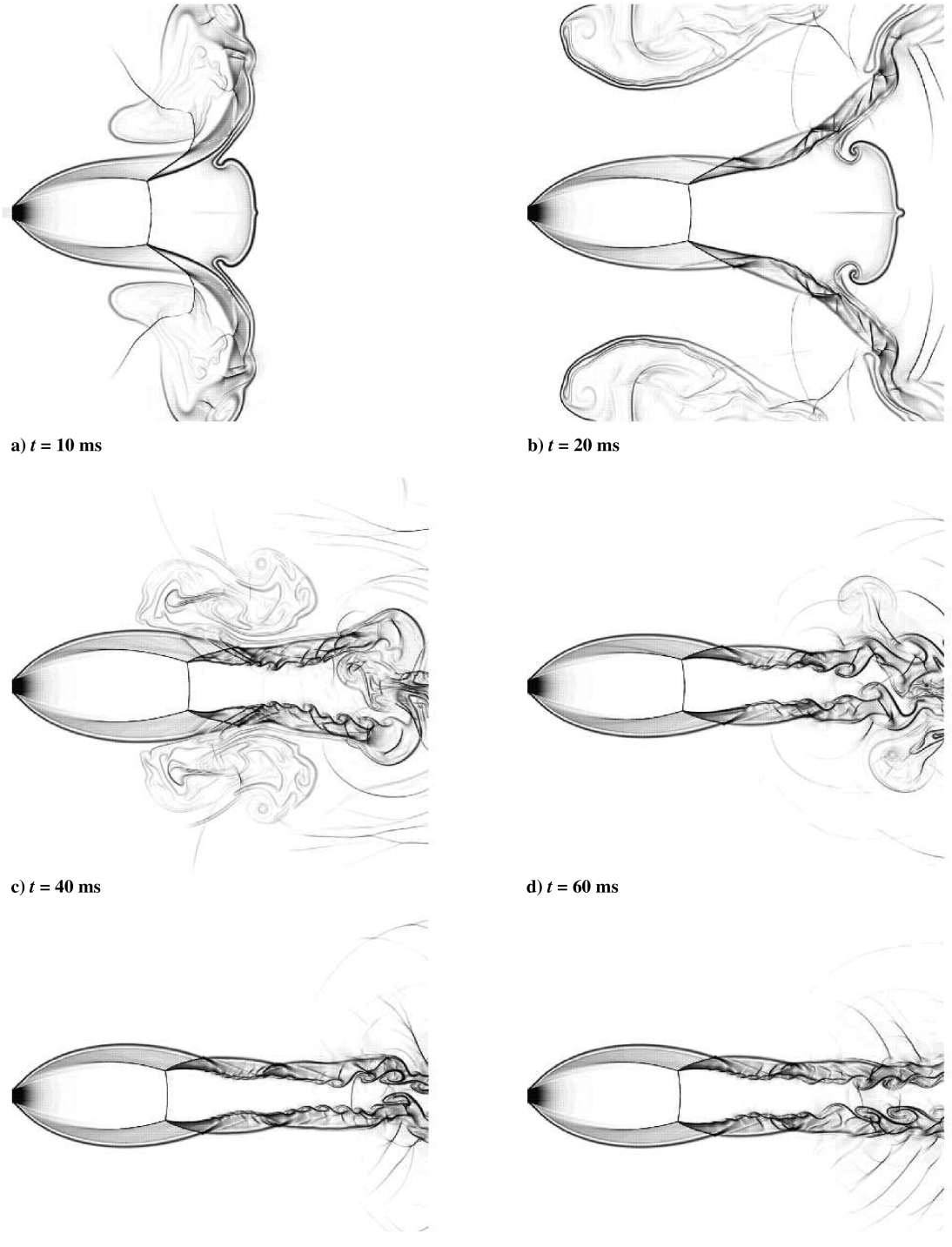

a) t **= 10 ms** **b)** t **= 20 ms**

c) t **= 40 ms** **d)** t **= 60 ms**

e) t **= 80 ms** **f)** t **= 100 ms**

Fig. 11 Development of flow for $p_4/p_1 = 50$, $\rho_4/\rho_1 = 28.74$, and $x_D/d = 0$.

The final set of comparisons involves the angle of vortex centers with respect to the diffraction corner and the Mach number of the vortex. Extracting the precise position of the vortex core is difficult, especially for higher Mach numbers, because it interacts with the slipstream, the secondary and tertiary shocks, and the contact discontinuity. The vortex appears to get compressed in the direction normal to the slipstream. Skews [17] alluded to the difficulties in identifying the vortex core from Schlieren images using the condition of a density minimum. Because of these difficulties, Skews did not present results for $M_s > 2$. From the computational results, however, the vortex core can be identified quite easily. Given the close proximity of the two shock waves and the contact discontinuity to the vortex, it is not obvious whether the location of a density minimum is the most suitable criterion for identifying the location of the vortex core. Furthermore, it was found that for higher Mach numbers, two density minima in close proximity to the vortex core could be observed. The vortex core identified by the density minimum did not agree well with the vortex core extracted from the velocity field. The two methods are compared with the experimentally determined vortex angle in Fig. 6e. Given the uncertainties in the experimental determination of the vortex core, the agreement for $M_s = 2$ is acceptable. The computational results for $M_s = 3$ and 4 indicate that the angular position obtained from the velocity field is consistently lower than that determined from the density minimum. Interestingly, the latter appears to reach a constant value for large Mach numbers, whereas the former does not. The computed Mach numbers of the vortex core (based on the location identified by inspecting the velocity field) are compared with the experiments in Fig. 6f. The agreement is excellent for $M_s = 2$ and acceptable for $M_s = 3$.

IV. Open-Ended Shock Tubes

Having demonstrated good agreement with experimental data at the early stages of the flow from an open-ended shock tube, we now turn our attention to later stages where an underexpanded jet forms at the open end. As discussed in the theory section, the later stages of the flow are influenced by the unsteadiness in the flow condition at the open end. To illustrate this effect, we consider three cases with different pressure ratios and diaphragm positions relative to the open end of the shock tube. These cases are summarized in Table 1. For the low-pressure ratio case, the Mach numbers of the shock wave, the flow behind the shock wave, and the flow behind the contact discontinuity are 1.53, 0.63, and 0.80, respectively. For the high-pressure ratio cases, the corresponding values are 2.41, 1.16, and 1.68. The geometric configuration and boundary conditions under consideration are depicted in Fig. 7. Shading indicates a region of uniform grid spacing. Numbers adjacent to the dashed arrows denote grid stretching in the direction of arrows. All boundaries are slip walls unless otherwise noted. For simplicity, we consider a planar configuration only. Throughout this section, t represents the time elapsed since the bursting of the diaphragm.

A. Low-Pressure-Ratio Case

For the low-pressure-ratio case, the well-known repeating barrel structure of moderately underexpanded jets is observed. The length of the first barrel, predicted to be about 2.7, compares reasonably well with the value 2.3 predicted by the approximate theory of Pack [31]. Given the difficulties of obtaining simple closed-form expressions for the evolution of the flow at the open end for subsonic flow behind the shock wave and the contact discontinuity, numerical simulations can be a useful tool to obtain insight. A numerically generated $x - t$ diagram based on the density gradient along the centerline of the shock tube is shown in Fig. 8. The shock wave, contact discontinuity, and expansion fan produced by the rupture of the diaphragm are labeled S, C, and $E1$, respectively. When the shock wave reaches the open end, an expansion fan labeled $E2$ is generated. The transmitted expansion fan generated by the interaction of $E2$ with the contact discontinuity is clearly visible and labeled $E3$. It can be seen that shortly after the interaction, the flow pattern at the open end becomes independent of time, indicating that sonic conditions are established and that $E3$ is accelerating the subsonic flow behind the contact discontinuity to supersonic conditions. This acceleration leads to the generation of an additional shock wave labeled $S2$ which reconciles the subsonic conditions behind the contact discontinuity with the supersonic conditions produced by $E3$. The evolution of the Mach number and pressure at the open end is shown in a later figure and will be discussed in more detail next.

B. High-Pressure-Ratio Cases

We compare the results to the experimental data of Bier and Schmidt [14]. The definitions of the flow features and the quantities to be compared are depicted in Fig. 9.

The overall development of the flow from the bursting of the diaphragm toward the steady state is visualized through numerically generated Schlieren pictures for $x_D/d = -1$ and $x_D/d = 0$ in Figs. 10 and 11, respectively. Up to about 20 ms, the flow evolution is similar regardless of the diaphragm position. It can be seen that the flowfield at 10 ms exhibits strong cross-streamwise components, probably induced by both the vortices and the deflection through the reflected shock. At 20 ms, the vortices have traveled further outward and back in the negative streamwise direction. Under the influence of

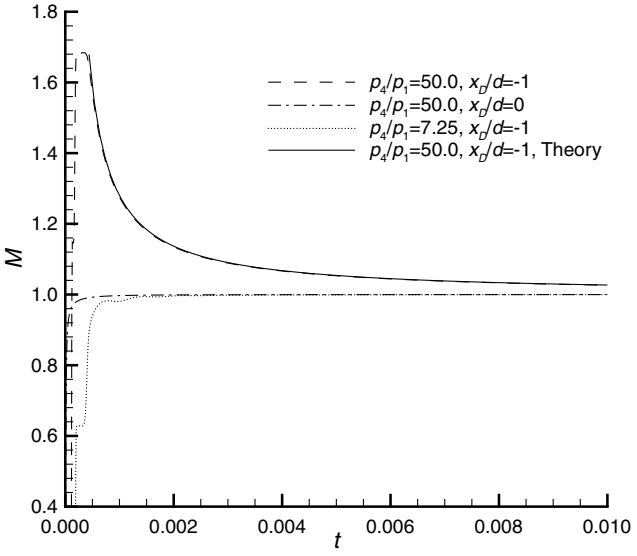

a) Mach number

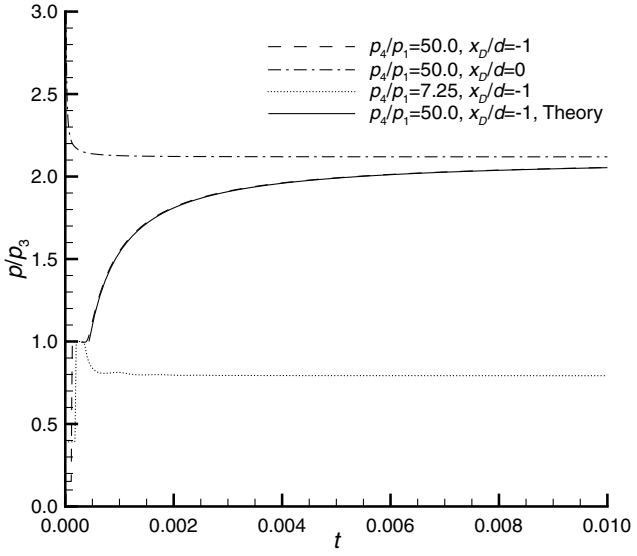

b) Pressure

Fig. 12 Evolution of Mach number and pressure at open end.

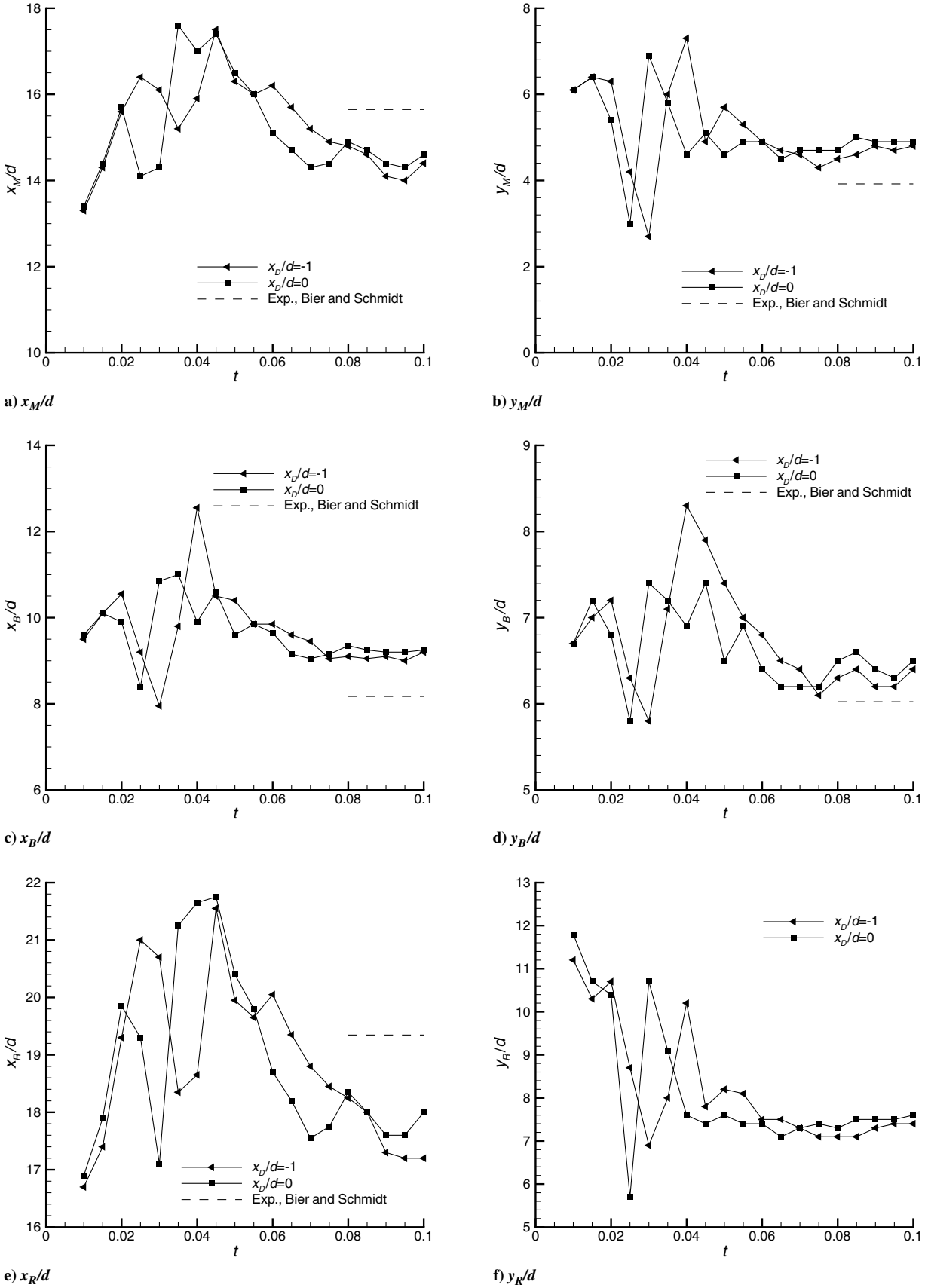

a) x_M/d b) y_M/d

c) x_B/d d) y_B/d

e) x_R/d f) y_R/d

Fig. 13 Comparison of computed temporal evolutions of quantities defined in Fig. 9 with experimental data for $x_D/d = -1$ and $x_D/d = 0$. No experimental data is available for y_R/d.

their induced motion and the jet entrainment, the vortices then move back toward the jet and appear to collide with the jet boundary. It seems reasonable to assume that this collision has a strong influence on the cross-streamwise extent of the Mach-disk shock. Following this collision, the vortices appear to be swept downstream and the well-known flow pattern of underexpanded jets is established.

The Mach number and pressure at the open end of the tube are depicted in Fig. 12. Several observations can be made. First, for

$x_D/d = -1$, the evolution shows the predicted behavior: the Mach number relaxes from M_3 to unity and the pressure increases from p_3 to the value given by Eq. (9). Second, the behavior follows very closely the theoretical evolution predicted by Eqs. (4) and (8). Third, for $x_D/d = 0$, the transient is essentially eliminated, again as predicted. (The very short transients which can be discerned in Fig. 12 are believed to be due to the finite thickness of the shock wave.) Fourth, the transient in the subsonic case is much shorter than for the supersonic case. The much shorter transient can be explained qualitatively by comparing Fig. 8 (illustrating the evolution of the flow for the subsonic case) to Fig. 3 (illustrating the evolution of the flow for the supersonic case). In the supersonic case, the conditions at the open end are approached only asymptotically. In the subsonic case, however, the transmitted expansion fan which accelerates the flow to supersonic conditions is located near the open end. In fact, the location of sonic conditions cannot be located anywhere but at the open end. Hence, the flow is accelerated almost instantaneously from the conditions behind the shock wave to sonic conditions. It is interesting to note that some oscillations are visible as the Mach number and pressure approach sonic conditions. The cause of these oscillations is not known, but may be due to the repeated reflections of the expansion waves from the open end.

The streamwise positions and cross-streamwise extents of the Mach-disk shock, barrel shock, and reflected shock are compared with the experimental data of Bier and Schmidt [14] in Fig. 13. The first observation to be made is that the development of the Mach-disk location and height for $x_D/d = -1$ is not simply that for $x_D/d = 0$ shifted in time by $x_D/u_s \approx 0.122$ ms. Up to a time of about 20 ms, the diaphragm position does not influence the Mach-disk location although first differences in the Mach-disk height can already be detected. Between 20 and 50 ms, major differences in the development of the Mach-disk location and height occur. For the Mach-disk location, the differences arise from opposite motion in the x direction. For example, although the Mach disk for $x_D/d = -1$ moves toward the open end, the opposite applies to the Mach disk for $x_D/d = 0$ and vice versa. For the Mach-disk height, the development is similar, except for a shift in time. After 50 ms, the overall trends of the Mach-disk position and height for $x_D/d = -1$ and $x_D/d = 0$ are approximately the same. At 10 ms, it can be seen that the numerical Mach-disk position is predicted to be closer to the open end than that observed in the experiment, whereas the Mach-disk height is predicted to be larger than that observed in the experiment. Figure 13a also demonstrates that the time scale on which a near-constant position of the Mach-disk shock is established is much longer than that required to establish the first barrel for the low-pressure-ratio case, consistent with the evolution of the Mach number and pressure at the open end.

The development of the barrel shock is similar to that of the Mach disk in that the largest deviations occur between 20 and 50 ms and that the overall trends after 50 ms are roughly the same. In contrast to the development of the Mach-disk position, the position of the barrel shock shows the same trends irrespective of the diaphragm position with the exception of a shift in time. Furthermore, it should be noted that the difference between the extrema of the barrel shock position and its extent is considerably larger for $x_D/d = -1$ than that for $x_D/d = 0$. The computed position and extent of the barrel shock overpredict the corresponding experimental values.

The evolution of the streamwise position and cross-streamwise extent of the reflected shock exhibits some similarities with that of the Mach-disk shock. This is not surprising, as an upstream or downstream shift in the Mach-disk position and an increase or decrease in the Mach-disk height must influence the reflected shock accordingly, assuming that the conditions immediately upstream of the reflected shock remain approximately constant. Hence, it is entirely consistent that the computed streamwise position of the reflected shock underpredicts the experimental value as for the Mach-disk shock. (No experimental data was presented by Bier and Schmidt [14] for the extent of the reflected shock.)

Two general observations can be made about the comparison of the computed results with the experimental data of Bier and Schmidt. First, the relatively large differences may be due, at least partly, to the difficulties in extracting the shock locations from experimentally obtained Schlieren pictures. Second, the streamwise position of the Mach-disk shock, the reflected shock, as well as the cross-streamwise extent of the barrel shock, exhibit oscillatory behavior at 100 ms. It is not clear if these oscillations would die out completely. The instability of the slipline is likely to send disturbances upstream because the flow behind the Mach-disk shock is subsonic. Hence, it is not inconceivable that some unsteadiness remains even for long times.

The loci of the streamwise location of the Mach-disk shock and the cross-streamwise extrema of Mach-disk shock, barrel shock, and reflected shock are shown in Fig. 14. The more extensive motion of the barrel shock for $x_D/d = -1$ can be seen clearly.

V. Conclusions

We have investigated the influence of the pressure ratio and the diaphragm location on the flow from open-ended shock tubes. In contrast to previous studies, in which attention was focused on the discharge of the shock wave from the shock tube, we have considered also the influence of the contact discontinuity and the expansion fan. If the pressure ratio is large enough to lead to supersonic flow behind the contact discontinuity, the flow at the open end relaxes from the conditions behind the contact discontinuity to sonic conditions once the tail of the expansion fan arrives at the open end. This relaxation process exhibits a number of interesting features. First, theory indicates that the time scale over which the flow relaxes to sonic conditions is nearly independent of the initial Mach number. Second, the time scale is much longer than that required by the acceleration of subsonic conditions behind the contact discontinuity to sonic conditions. This difference was explained by the nearly instantaneous acceleration in the transmitted expansion fan caused by the refraction of the reflected expansion wave at the contact discontinuity for subsonic flow behind the contact discontinuity. The relaxation process was shown to influence the evolution of the Mach-

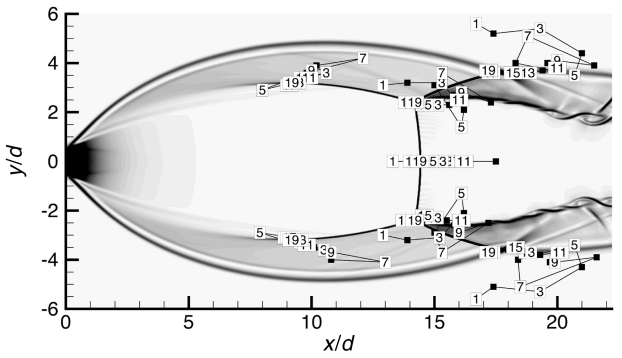

a) $x_D/d = -1$

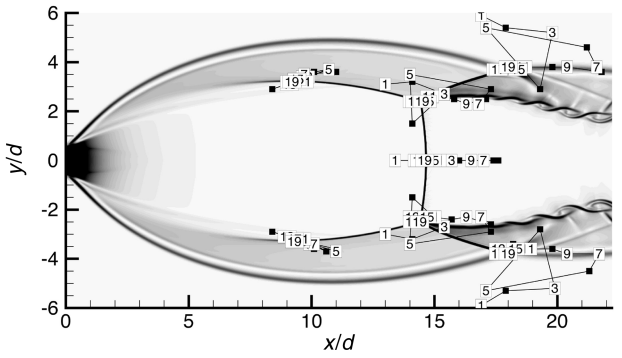

b) $x_D/d = 0$

Fig. 14 Loci of cross-streamwise extrema of Mach-disk shock, barrel shock, and reflected shock for $p_4/p_1 = 50$, $\rho_4/\rho_1 = 28.74$, superimposed on numerically generated Schlieren pictures at $t = 100$ ms. Labels in boxes denote mapping to time; label index i is equivalent to time $t = 10^{-2}[1 + (i - 1)/2]$.

disk shock, the barrel shock, and the reflected shock wave in an underexpanded jet.

Acknowledgments

The first author was funded by the U.S. Department of Energy through the University of California under Subcontract No. B341494 while part of this work was performed at the Center for Simulation of Advanced Rockets (CSAR) at the University of Illinois at Urbana–Champaign. This work was supported by the National Science Foundation through Grant No. 0609712. Computing Resources were provided by the CSAR and the National Center for Supercomputing Applications.

References

[1] Bradley, J. N., *Shock Waves in Chemistry and Physics*, Wiley, New York, 1962.
[2] Gaydon, A. G., and Hurle, I. R., *Shock Tube in High-Temperature Chemical Physics*, Reinhold, New York, 1963.
[3] Glass, I. I., and Sislian, J. P., *Nonstationary Flows and Shock Waves*, Clarendon, Oxford, England, U.K., 1994.
[4] Alpher, R. A., and White, D. R., "Flow in Shock Tubes with Area Change at the Diaphragm Section," *Journal of Fluid Mechanics*, Vol. 3, No. 2, 1958, pp. 457–470.
[5] Sugiyama, H., "Performance Study of Shock Tubes with Area Change at the Diaphragm Section," *Bulletin of the Japan Society of Mechanical Engineers*, Vol. 26, No. 216, 1983, pp. 958–963.
[6] Emanuel, G., Satyanand, U. S., and Lu, F. K., "Performance of a Shock Tube with a Large Area Contraction," *AIAA Journal*, Vol. 43, No. 9, 2005, pp. 1995–1999.
[7] Kim, H. D., and Setoguchi, T., "Study of the Discharge of Weak Shocks from an Open End of a Duct," *Journal of Sound and Vibration*, Vol. 266, No. 5, 1999, pp. 1011–1028.
[8] Kim, H. D., Kweon, Y. H., Setoguchi, T., and Aoki, T., "Weak Shock Reflection from an Open End of a Tube with a Baffle Plate," *Proceedings of the Institution of Mechanical Engineers Part C, Mechanical Engineering Science*, Vol. 217, No. 6, 2003, pp. 651–659.
[9] Phan, K. C., and Stollery, J. L., "Effect of Suppressors and Muzzle Brakes on Shock Wave Strength," *Proceedings of the 14th International Symposium on Shock Tubes and Waves*, Sydney Shock Tube Symposium Publishers, Sydney, Australia, 1984, pp. 519–526.
[10] Schmidt, E. M., and Duffy, S. J., "Noise from Shock Tube Facilities," AIAA Paper 85-0049, Jan. 1985.
[11] Rudinger, G., "On the Reflection of Shock Waves from an Open End of a Duct," *Journal of Applied Physics*, Vol. 26, No. 8, 1955, pp. 981–993.
[12] Rudinger, G., "Improved Wave Diagram Procedure for Shock Reflection from an Open End of a Duct," *Journal of Applied Physics*, Vol. 26, No. 11, 1955, pp. 1339–1341.
[13] Adamson, T. C., Jr., and Nicholls, J. A., "On the Structure of Jets from Highly Underexpanded Nozzles into Still Air," *Journal of the Aero/Space Sciences*, Vol. 26, No. 1, 1959, pp. 16–24.
[14] Bier, K., and Schmidt, B., "Zur Form der Verdichtungsstösse in frei expandierenden Gasstrahlen," *Zeitschrift für Angewandte Physik*, Vol. 13, No. 11, 1961, pp. 493–500.
[15] Whitham, G. B., "New Approach to Problems of Shock Dynamics, Part 1: Two-Dimensional Problems," *Journal of Fluid Mechanics*, Vol. 2, March 1957, pp. 145–171.
[16] Skews, B. W., "Shape of a Diffracting Shock Wave," *Journal of Fluid Mechanics*, Vol. 29, No. 2, 1967, pp. 297–304.
[17] Skews, B. W., "Perturbed Region Behind a Diffracting Shock Wave," *Journal of Fluid Mechanics*, Vol. 29, No. 4, 1967, pp. 705–719.
[18] Hillier, R., "Computation of Shock Wave Diffraction at a Ninety Degrees Convex Edge," *Shock Waves*, Vol. 1, No. 2, 1991, pp. 89–98.
[19] Hillier, R., "Numerical Modelling of Shock Wave Diffraction," *Shock Waves @ Marseille*, edited by Brun, R. and Dumitrescu, L. Z., Springer–Verlag, Berlin, 1995, pp. 17–26.
[20] Baird, J. P., "Supersonic Vortex Rings," *Proceedings of the Royal Society of London A*, Vol. 409, No. 1836, 1987, pp. 59–65.
[21] Sun, M., and Takayama, K., "Vorticity Production in Shock Diffraction," *Journal of Fluid Mechanics*, Vol. 478, March 2003, pp. 237–256.
[22] Chang, K.-S., and Kim, J.-K., "Numerical Investigation of Inviscid Shock Wave Dynamics in an Expansion Tube," *Shock Waves*, Vol. 5, Nos. 1–2, 1995, pp. 33–45.
[23] Jiang, Z., Takayama, K., Babinsky, H., and Meguro, T., "Transient Shock Wave Flows in Tubes with a Sudden Change in Cross Section," *Shock Waves*, Vol. 7, No. 3, 1997, pp. 151–162.
[24] Yu, Q., and Grönig, H., "Shock Waves from an Open-Ended Shock Tube with Different Shapes," *Shock Waves*, Vol. 6, No. 5, 1996, pp. 249–258.
[25] Haselbacher, A., "WENO Reconstruction Method for Unstructured Grids Based on Explicit Stencil Construction," AIAA Paper 2005-0879, Jan. 2005.
[26] Owczarek, J. A., *Fundamentals of Gas Dynamics*, International Textbook, Scranton, PA, 1964.
[27] Rudinger, G., "Note on the Use of the Shock Tube as an Intermittent Supersonic Wind Tunnel," *Physical Review*, Vol. 75, No. 12, 1949, pp. 1948–1949.
[28] Billington, I. J., and Glass, I. I., "On the One-Dimensional Refraction of a Rarefaction Wave at a Contact Surface," Univ. of Toronto Inst. of Aerophysics Rept. 31, 1955.
[29] Glaz, H. M., Colella, P., Glass, I. I., and Deschambault, R. L., "Numerical Study of Oblique Shock Wave Reflections with Experimental Comparison," *Proceedings of the Royal Society of London A*, Vol. 398, No. 1814, 1985, pp. 117–140.
[30] Bazhenova, T. V., Gvozdeva, L. G., Komarov, V. S., and Sukhov, B. G., "Investigation of a Strong Shock Wave Diffraction at Convex Corners," *Izvestiya Akademii Nauk SSSR Mekhanika Zhidkostii Gaza*, Vol. 4, July–Aug. 1973, pp. 122–134.
[31] Pack, D. C., "Note on Prandtl's Formula for the Wave-Length of a Supersonic Gas Jet," *Quarterly Journal of Mechanics and Applied Mathematics*, Vol. 3, Pt. 2, 1950, pp. 173–181.

G. Candler
Associate Editor